URSI GASS 2021, Rome, Italy, 28 August - 4 September 2021

Through-the-Wall Imaging by means of a Hybrid Inverse-Scattering Procedure

Andrea Randazzo* (1), Cristina Ponti(2), Valentina Schenone(1), Alessandro Fedeli(1),
Claudio Estatico(3), Paolo D'Atanasio(4), Matteo Pastorino(1), and Giuseppe Schettini(2)
(1) Department of Electrical, Electronic, Telecommunications Engineering and Naval Architecture,
University of Genoa, 16145 Genoa, Italy; e-mail: valentina.schenone@edu.unige.it,
{alessandro.fedeli; matteo.pastorino; andrea.randazzo}@unige.it
(2) Department of Engineering, "Roma Tre" University, 00146 Rome, Italy;
e-email: {cristina.ponti; giuseppe.schettini}@uniroma3.it
(3) Department of Mathematics, University of Genoa, 16145 Genoa, Italy; e-mail: estatico@dima.unige.it
(4) Italian National Agency for New Technologies, Energy and Sustainable Economic Development,
Casaccia Research Center, 00123 Rome, Italy; e-mail: paolo.datanasio@enea.it

Abstract

In this work, an inverse-scattering technique for through-the-wall imaging is presented and validated against experimental data. The inverse-scattering scheme is developed in variable-exponent Lebesgue spaces, where a delay-and-sum beamforming approach is preliminary applied to build the exponent function. Measurements are collected as time-domain data in a laboratory environment, under a multi-illumination and multi-view approach. Processing of the data is performed in the frequency-domain, by application of the Fast Fourier Transform, and extracting the scattered fields at several frequencies in order to improve the reconstruction capabilities. The obtained results confirm the successful imaging of both high- and low-reflectivity targets in the inspected scenario.

1 Introduction

Through-the-Wall (TW) radar is a technique for the detection of targets hidden behind a wall by using microwave fields, developed for applications of surveillance, security, rescue and fire succor [1]. Processing of the measured data aims at a localization of the target, as well as at an imaging of the investigated scene, a procedure that is also known as Through-the-Wall Imaging (TWI) [2]. Several approaches have been proposed, which are mainly developed with beamforming schemes [3] or linearized inverse-scattering solutions [4], [5]. A qualitative imaging of the target is usually provided, which allows identifying the target shape and size, and the detection of boundaries.

In this framework, an important role is played by a correct modeling of the propagation in TW environments [6], [7]. Indeed, the scattered fields suffer from multipaths and attenuation losses, which are caused by interaction with the wall's boundaries and by dielectric properties of the wall material. Therefore, without a proper implementation of the TWI algorithms in TW backgrounds, the quality of the reconstruction may be strongly impaired, resulting in spurious images and artifacts.

In this paper, the TWI problem is addressed by means of a hybridized algorithm that combines a Delay and Sum (DAS) approach [8] and an inverse-scattering scheme developed in variable-exponent Lebesgue spaces [9]. The role of the DAS is to provide a map of the exponent function from the available measured data. As to the inversion scheme, it is based on a linearized formulation relying on the use of a proper Green's function for modeling the through-wall background. The algorithm is validated against measured data collected in a laboratory environment with a pulsed Ground Penetrating Radar (GPR). A Fast Fourier Transform is applied to the time-domain data to obtain the scattered fields in input to the imaging method. Data at several frequencies are considered, thus enhancing the reconstruction capabilities of the algorithm.

The paper is organized as follows: in Section 2, the TWI approach is briefly outline; in Section 3, application of the inversion scheme to experimental data is presented; conclusions are drawn in Section 4.

2 Overview of the Through-the-Wall Modeling and Imaging Approach

Figure 1 shows a schematic representation of the considered TWI configuration. S antennas are uniformly spaced along a probing line of length L_s located in front of a wall with thickness l_w and complex dielectric permittivity ϵ_w. In particular, when the antenna in the s-th position ($s = 1, \dots, S$) is used in transmission (TX) mode, the scattered field is collected by $M = S - 1$ receiving (RX) antennas located in the remaining positions.

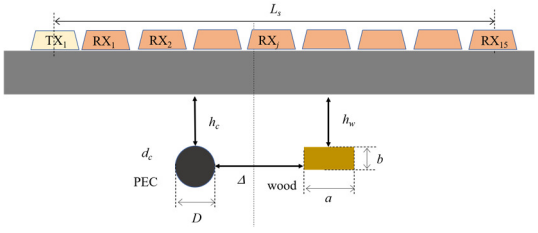

Figure 1. Configuration of the considered TWI problem.

In the developed approach, the TX antennas are modeled as ideal line-current sources, whereas the RX elements as ideal probing points. Under such conditions, and considering a linear approximation of the scattering equations, the scattered field produced by the interaction between the targets in the investigation domain D and the s-th incident field is approximately modeled as [5]

$$e_{sct}^{s}(\mathbf{r}_{RX}^{s,m},\omega_f) \cong \beta_s \int_D \gamma(\mathbf{r}')g_{tw}(\mathbf{r}',\mathbf{r}_{TX}^{s},\omega_f)g_{tw}(\mathbf{r}_{RX}^{s,m},\mathbf{r}',\omega_f)d\mathbf{r}' \quad (1)$$

where β_s is an amplitude factor depending on the source, ω_f is the working angular frequency (an $e^{j\omega t}$ time dependence is assumed and omitted, and F different frequency values are considered), $\mathbf{r}_{TX}^{s}$ is the position of the TX antenna, $\mathbf{r}_{RX}^{s,m}$ is the location of the m-th receiving point for the s-th view, and γ is the contrast function. It is worth remarking that, when dealing with weak scatterers, γ effectively provides information about the dielectric contrast, whereas for strong scatterers (e.g., metallic targets) it only allows obtaining information about shape and location.

Equation (1) holds true for every measurement location, and in discretized form becomes $\underline{e}_{sct}^{f,s} = [G_{tw}^{f,s}]\underline{\gamma}$, where $\underline{e}_{sct}^{f,s}$ is an array containing all the scattered field measurements for the f-th frequency and s-th illumination, $[G_{tw}^{f,s}]$ is a matrix containing the integrals of the Green's functions, and $\underline{\gamma}$ contains the discretized contrast function (the investigation domain D is divided into N square subdomains in which γ assumes constant values). By stacking all the equations for the F available frequencies and S illuminations, the following discrete model is finally obtained:

$$\underline{e}_{sct} = [G_{tw}]\underline{\gamma} \quad (2)$$

Equation (2) needs to be solved in order to retrieve the unknown $\underline{\gamma}$ from the scattered field measurements $\underline{e}_{sct}$. To this end, a hybrid inversion procedure, combining a beamforming scheme with an inverse-scattering technique has been developed. In the first step, a qualitative image is obtained by applying a multi-static DAS technique [8], i.e., an image Υ_{DAS} is built as

$$\Upsilon_{DAS}(\mathbf{r}) = \sum_{f,s,m} e_{sct}^{s}(\mathbf{r}_{RX}^{s,m},\omega_f)e^{j\omega_f\tau(\mathbf{r},\mathbf{r}_{TX}^{s},\mathbf{r}_{RX}^{s,m})} \quad (3)$$

where $\tau(\mathbf{r},\mathbf{r}_{TX}^{s},\mathbf{r}_{RX}^{s,m})$ is the round-trip delay required by the wave generated by the TX antennas to reach the generic point $\mathbf{r}$ and to return to the RX antenna. Such a delay takes into account the presence of the wall and is numerically computed by exploiting the Fermat principle.

The second step consist in the solution of (2) by means of a Landweber-like iterative method performing a regularization in the framework of the variable-exponent $L^{p(\cdot)}$ spaces [9]. In particular, the exponent function defining the adopted space $L^{p(\cdot)}$ is obtained from the DAS image as

$$p(\mathbf{r}) = p_{min} + \Delta p \frac{|\Upsilon_{DAS}(\mathbf{r})|}{\max_{\mathbf{r}\in D_{inv}}|\Upsilon_{DAS}(\mathbf{r})|} \quad (4)$$

where p_{min} and Δp are parameters defining the range of admissible values of this function.

3 Experimental results

An example of validation of the algorithm introduced in Section 2 against experimental measurements is reported here. The schematic view of the laboratory setup is shown in Figure 2. The targets are a circular-cross section metallic cylinder of diameter $D = 10$ cm, and a wood cylinder with rectangular cross section of sides $a \times b$, with $a = 16$ cm and $b = 8$ cm, placed behind a wall of thickness $l_w = 25$ cm. The distance of the metallic cylinder from the wall is $h_c = 50$ cm, whereas the wood cylinder is located at a lower distance $h_w = 40$ cm. The horizontal separation between the two targets is $\Delta = 60$ cm, as described in the layout of Figure 1. Measured data are collected in the time-domain with a commercial GPR equipment. The TX and RX antennas are scanned in a multi-view and multi-illumination mode in $S = 16$ positions taken along a line parallel to the wall, and of length $L_S = (S-1)$, where $d = 14.5$ mm is the spacing among antennas. The TX antenna radiates a pulsed waveform with central frequency $f_c = 1$ GHz.

The field collected in the presence of the wall alone, i.e., without targets, is subtracted to the total field measured in the presence of the two objects, to remove the response of the wall. Figure 3 shows the obtained B-scan radargram, evaluated for the TX antenna in the position $s = 9$. Wall reflections are still visible, due to uncertainties in the positions of the antennas in the two measurements (with and without target) and measurement errors. At later arrival times, two hyperbolas are displayed: a stronger one is relevant to the scattered field by the metallic cylinder, and a weaker one by the wood target.

FFT is applied to time-domain measurements to derive frequency domain data. The inversion algorithm is applied using $F = 31$ frequencies, equally distributed in the interval $[0.5, 2]$ GHz, and setting the following parameters: maximum number of iterations, $I_{max} = 100$; threshold on the relative variation of the residual, 0.01, minimum exponent value, $p_{min} = 1.4$; range of the exponent function, $\Delta p = 0.6$.

Figure 2. Laboratory setup.

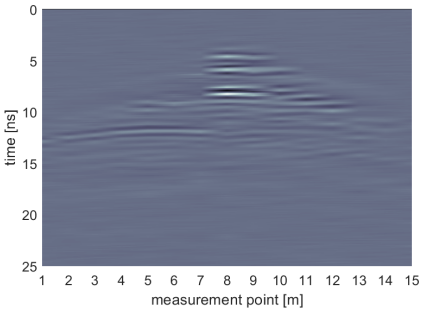

Figure 3. B-scan radargram with the TX antenna in position $s = 9$.

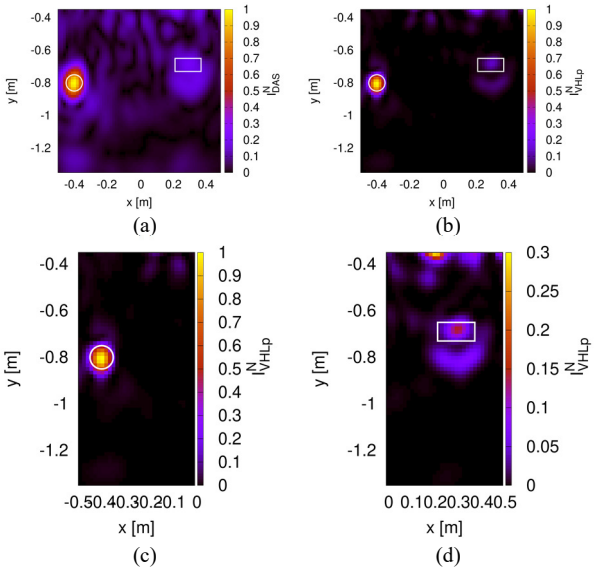

Figure 4. Reconstructed images of the off-centered metallic and wood targets. (a) DAS and (b) hybrid variable exponent methods; zoom on the (c) left and (d) right parts of the investigation domain.

The reconstructed images are reported in Figure 4. In particular, Figure 4(a) shows the DAS image, where a significant background noise is present, and sizes of the targets are not correctly estimated. A much clearer image is instead returned in the final results reported in Figure 4(b). The metallic target is correctly estimated in terms of position and size, whereas the reconstruction of the wood target, which is more challenging due to the low dielectric contrast with respect to the background, is less visible in the investigated scene. A zoom on metallic and wood cylinder is performed in Figure 4(c) and Figure 4(d), respectively. From these figures, it can be observed that also the wood target is correctly localized.

4 Conclusion

A hybrid through-the-wall imaging approach, relying on the use of a variable-exponent Lebesgue space regularization method combined with a beamforming technique for the creation of the norm exponent function, has been considered in this paper. The developed approach has been validated on experimental data, showing very good reconstruction capabilities for both metallic and dielectric targets.

5 Acknowledgements

This work was partially supported by the Italian Ministry for Education, University, and Research under the project PRIN2015 U-VIEW, grant number 20152HWRSL.

6 References

1. M. G. Amin, Ed., *Through-the-Wall Radar Imaging*. Boca Raton, FL: CRC Press, 2011.

2. M. Pastorino and A. Randazzo, *Microwave Imaging Methods and Applications*. Boston, MA: Artech House, 2018.

3. B. Yektakhah and K. Sarabandi, "All-directions through-the-wall imaging using a small number of moving omnidirectional bi-static FMCW transceivers," *IEEE Transactions on Geoscience and Remote Sensing*, **57**, 5, May 2019, pp. 2618–2627, doi: 10.1109/TGRS.2018.2875695.

4. F. Soldovieri and R. Solimene, "Through-wall imaging via a linear inverse scattering algorithm," *IEEE Geoscience and Remote Sensing Letters*, **4**, 4, October 2007, pp. 513–517, doi: 10.1109/LGRS.2007.900735.

5. R. Solimene, F. Soldovieri, G. Prisco, and R. Pierri, "Three-dimensional through-wall imaging under ambiguous wall parameters," *IEEE Transactions on Geoscience and Remote Sensing*, **47**, 5, May 2009, pp. 1310–1317, doi: 10.1109/TGRS.2009.2012698.

6. A. Fedeli, M. Pastorino, C. Ponti, A. Randazzo, and G. Schettini, "Through-the-wall microwave imaging: Forward and inverse scattering modeling," *Sensors*, **20**, 10, January 2020, p. 2865, doi: 10.3390/s20102865.

7. C. Ponti and S. Vellucci, "Scattering by conducting cylinders below a dielectric layer with a fast noniterative approach," *IEEE Transactions on Microwave Theory and Techniques*, **63**, 1, January 2015, pp. 30–39, doi: 10.1109/TMTT.2014.2376553.

8. F. Boero, A. Fedeli, M. Lanini, M. Maffongelli, R. Monleone, M. Pastorino, A. Randazzo, A. Salvadè, and A. Sansalone, "Microwave tomography for the inspection of wood materials: imaging system and experimental results," *IEEE Transactions on Microwave Theory and Techniques*, **66**, 7, July 2018, pp. 3497–3510, doi: 10.1109/TMTT.2018.2804905.

9. I. Bisio, C. Estatico, A. Fedeli, F. Lavagetto, M. Pastorino, A. Randazzo, and A. Sciarrone, "Variable-exponent Lebesgue-space inversion for brain stroke microwave imaging," *IEEE Transactions on Microwave Theory and Techniques*, **68**, 5, May 2020, pp. 1882–1895, doi: 10.1109/TMTT.2019.2963870.